[Article ID] 1003- 6326(2002)05- 0829- 04

Correlation between liquid structure and γ_2-phase precipitation of Cu-Al-Ni shape memory alloys ①

PAN Xue-min(潘学民), BIAN Xiu-fang(边秀房), SUN Jing-qin(孙景芹), WANG Wei-min(王伟民)
(Key Laboratory of Liquid Structure and Heredity of Materials, Ministry of Education, Shandong University, Ji'nan 250061, China)

[Abstract] $Cu_{71}Al_{25}Ni_4$(mole fraction, %) shape memory alloy ribbons exhibit a good shape memory effect, which were prepared by melt-spinning technique. The microstructure of the as-spun ribbons was identified by D/Max-rA X-ray diffractometer. The order degree of martensite increases with decreasing liquid quenching temperature at the same quenching rate. The liquid structure of $Cu_{75}Al_{25}$ and $Cu_{71}Al_{25}Ni_4$ was investigated using X-ray diffraction method. The distinct pre-peaks have been found in front of main peaks of the structure factors. The pre-peak increases intensity with decreasing temperature or adding Ni. Gaussian peaks decomposing radial distribution function (RDF) indicated that Cu-Al distance is anomalously short. These results suggest that a strong interaction between Cu and Al is favorable to form β-phase-like clusters, which leads to chemical medium-range ordering in melt. This promotes formation of order martensite and suppresses γ_2-phase precipitation.

[Key words] CuAlNi alloy; liquid structure; shape memory alloy; X-ray diffraction
[CLC number] TG 139 [Document code] A

1 INTRODUCTION

Cu-base shape memory alloys (SMA) are commercially attractive systems for the practical exploitation of the shape memory effect (SME) and stand next in line to the Ni-Ti base alloys as suitable alloys for shape memory application because of their lower cost. Many studies have been carried out on the various aspects of SME in Cu-base alloys system[1~4], including crystallography and morphology of martensite, transformation temperature and phase stability, aging effect, and SME property. But very few experiments have been carried out on liquid structure of SMA. More and more facts have clearly revealed that the structure and properties of the solid state are related to the structure of the liquid. It is concluded that some small structure units in liquid are the heredity factors of solid when it is solidified[5]. In addition, it is known that rapid solidification can better reveal the relation between the structure of the melt and the microstructure of the solid. In present work, CuAlNi shape memory alloys ribbons were fabricated by melt-spinning technique, which is one of techniques for rapid solidification. The microstructure and hardness of ribbons and the liquid structure of melt were investigated.

2 EXPERIMENTAL

The alloys of $Cu_{75}Al_{25}$ and $Cu_{71}Al_{25}Ni_4$ (mole fraction, %) were prepared by melting the pure metals (99.99%, mass fraction) in an induction furnace, then poured into permanent mould and the cylindrical specimens with 10 mm in diameter were obtained. The specimens were put in the quartz tube with narrow slit and then equipped with melt-spinning apparatus and melt spun ribbons were fabricated. The phase of the as-spun ribbons was identified by Shimazu XD-3A X-ray diffractometer. The liquid structure of melt has been investigated with high temperature X-ray diffraction, using an θ-θ diffractometer (Mo K_α). Please refer to Refs.[6~8] for the detail of the data processing.

3 RESULTS AND DISCUSSION

The ribbons were 8~ 10 mm in width and ~ 80 μm in thickness. The as-spun ribbon bent at ambient temperature returns to its original shape as temperature rising up to about 150 ℃. This result shows that the as-spun ribbon exhibits a good shape memory effect.

Fig. 1 shows X-ray diffraction patterns of the as-spun ribbons of $Cu_{71}Al_{25}4_4$ alloys at different liquid quenching temperatures when the rotation rate is 200 r/min. The (111) and (019) are the characteristic superlattice peaks due to DO_3 order and the other peaks are mainly the fundamental reflection peaks of martensite.

The degree of DO_3 long-range order S can be estimated through[3]

$$S = \left| \frac{(I_s/I_f)_{exp}}{(I_s/I_f)_{cal}} \right|^{1/2} \quad (1)$$

① [Foundation item] Project (50071028) supported by the National Natural Science Foundation of China and (L2000F01) supported by the Natural Science Foundation of Shandong Province, China [Received date] 2001- 10- 08; [Accepted date] 2002- 03- 07

where I_s represents the intensity of superlattice

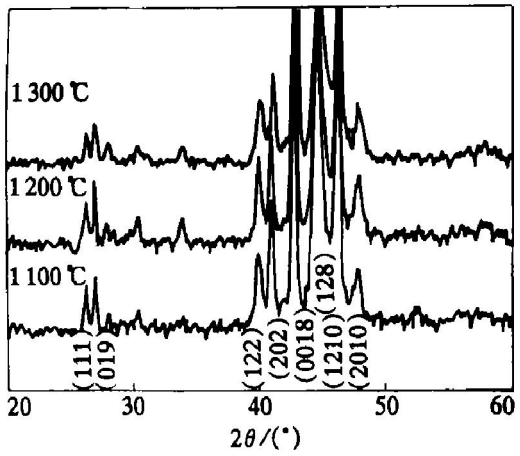

Fig. 1 XRD spectra for $Cu_{71}12_{25}Ni_4$ ribbons

reflection peak; I_f represents the intensity of fundamental reflection peak; $(I_s/I_f)_{exp}$ is ratio of the two experimental intensity; $(I_s/I_f)_{cal}$ is theoretical ratio of value corresponding to complete order structure. In same phase state, the equation can be obtained as follows

$$\frac{S'}{S''}=\left|\frac{(I_s/I_f)'_{exp}}{(I_s/I_f)''_{exp}}\right|^{1/2} \quad (2)$$

Thus, variation in the order degree of martensite can be known by comparing the ratio of the (111) or (019) to the fundamental reflection peak at different liquid quenching temperatures. From Fig. 1, it is obvious that the intensity of superlattice peaks increases with decreasing liquid quenching temperature. This suggests order degree of as-spun martensite increases with decreasing liquid quenching temperature.

The ratio of intensity of (111) and (019) to (0018) of the as-spun ribbons at different rotation rates are given in Table 1. The (0018) is a fundamental reflection peak of martensite. A remarkable feature noted by Cantor is that the cooling rate in melt spinning can be represented by a simple relation of the type: $R=\alpha V$, where R is the cooling rate, V is the wheel velocity and α is a constant ($=1.2\times10^4$ K/m)[5, 9]. In the present experiment, variation in thickness of all ribbons is so small that the influence of thickness on cooling rate can be ignored. From Table 1, the order degree of martensite decreases with increasing the rotation rate due to the higher cooling rate resulting in ordering of martensite incomplete. When the liquid quenching temperature is 1 100 ℃, the (111) intensity relative to the (0018) of the as-spun ribbons at the rotation rate of 300 r/min is 0.16; when the liquid quenching temperature is 1 300 ℃, the (111) intensity relative to the (0018) of the as-spun ribbons at the rotation rate of 50 r/min is 0.13. The former is higher than the latter. This suggests that the liquid quenching temperature has very important influence on order degree of as-spun ribbons.

In Fig. 2, curve 1 shows the Vickers hardness varies with the liquid quenching temperature and curve 2 shows the Vickers hardness varies with the rotation rate. It shows that the Vickers hardness of as-spun ribbons decreases with decreasing liquid quenching temperature at the same rotation rate and with increasing rotation rate at the same liquid quenching temperature. Therefore, the Vickers hardness of ribbons is related not only to the cooling rates but also to the quenching temperature closely.

Fig. 3 shows the Vickers hardness varies with the aging temperature for ribbons obtained at various liquid quenching temperatures as the aging time is 15 min. The hardness of ribbons changed significantly during

Table 1 XRD relative intensity of superlattice peaks for SMA ribbons at different rotation rates

Rotation rate/(r·min^{-1})	1 300 ℃		1 100 ℃	
	hkl	I_s/I_f	*hkl*	I_s/I_f
50	(111)	13%	(111)	19%
	(019)	18%	(019)	19%
200	(111)	11%	(111)	18%
	(019)	13%	(019)	21%
300	(111)	8%	(111)	16%
	(111)	8%	(019)	19%

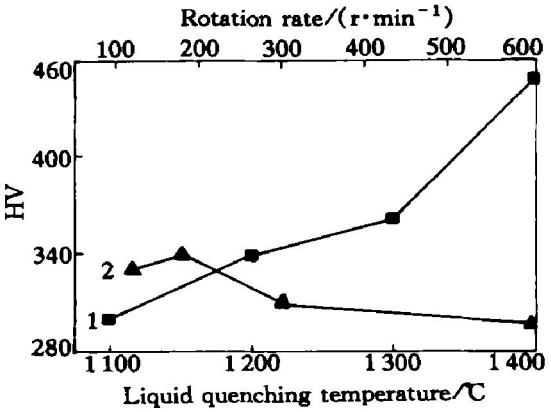

Fig. 2 Changes in Vickers hardness with rotation rate and quenching temperature
■ —At the same rotation rate(180 r/min)
▲ —At the same quenching temperature(1 200 ℃)

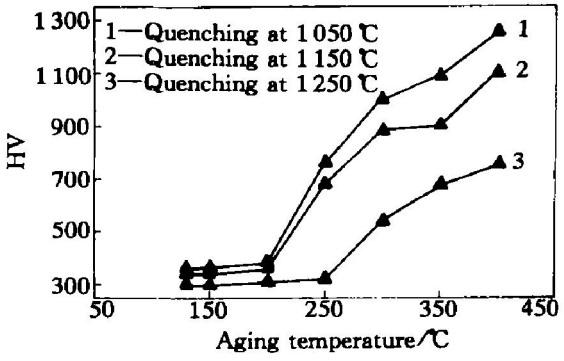

Fig. 3 Relation between aging temperature and micro-Vickers hardness of as-spun ribbons

the aging. This was caused by the precipitation of γ_2 phase. The point at which the hardness begins to rise was thought to be corresponded to the temperature where γ_2 phase precipitated, and the shift to higher temperature was detected when liquid quenching temperature was decreased.

The total structure factors of liquid $Cu_{75}Al_{25}$ alloy are shown in Fig. 4. A distinct pre-peak has been found in front of main peak of the structure factors. As we know, the curves take on a shape of parabola ahead the main peak in the structure factors of molten Al and Cu[7]. So appearance of the pre-peak in the structure factor of molten $Cu_{75}Al_{25}$ must be due to Cu-Al interaction. The total structure factors of liquid $Cu_{71}Al_{25}Ni_4$ alloy are shown in Fig. 5. The pre-peak increases after addition of Ni. The intensity of pre-peaks is strengthened with decreasing temperature, as shown in Fig. 4 and Fig. 5. For the structure factor curve, the ratio of the pre-peak area (the integrated intensity of the curve) to the total area of the curve can reflect the ratio of the structure corresponding to the pre-peak in melt[10]. So the amount of the structure corresponding to the pre-peak in melt increases with decreasing temperature and addition of Ni.

The first peak of radial distribution function (RDF) $4\pi\gamma^2\rho(\gamma)$ of $Cu_{75}Al_{25}$ and $Cu_{71}Al_{25}Ni_4$ were fitted by three Gausian functions, as shown in Fig. 6 and Fig. 7. The positions and areas for the three sub-peaks are listed in Table 2. Since the area of the first sub-peak increases with addition of Ni(which is small atom) and Cu in two alloy systems, it is reasonable to assign the first sub-peak to the Cu-Al correlation. The

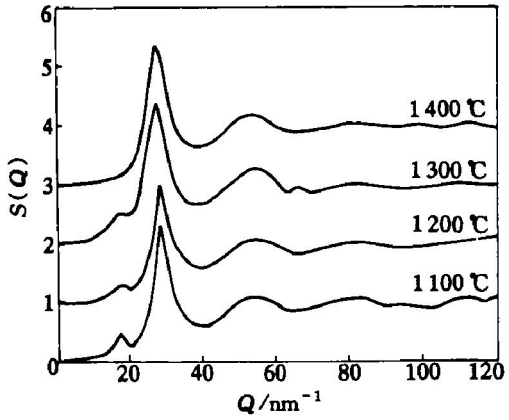

Fig. 4 Total structure factors of liquid $Cu_{75}Al_{25}$ alloy

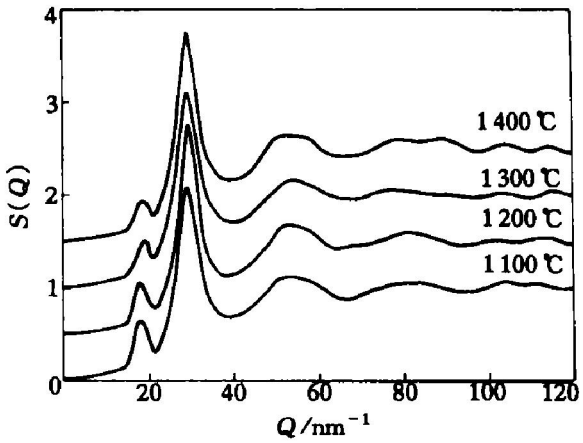

Fig. 5 Total structure factors of liquid $Cu_{71}A_{25}Ni_4$ alloy

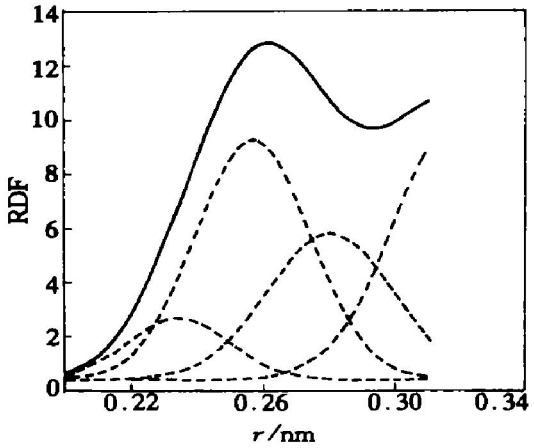

Fig. 6 The first peak of RDF of $Cu_{75}Al_{25}$ fitted by three Gaussian function

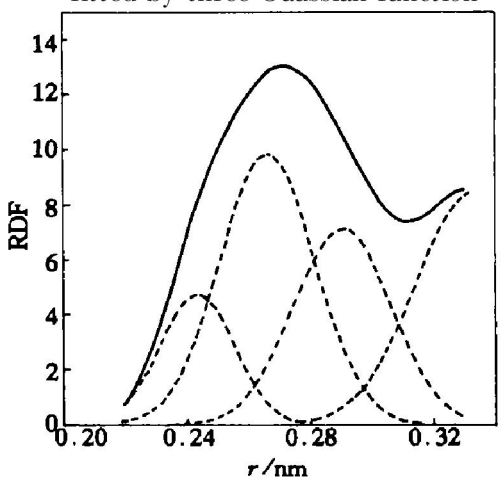

Fig. 7 The first peak of RDF of $Cu_{71}Al_{25}Ni_4$ fitted by three Gaussian function

Table 2 Positions and areas of sub-peaks of RDF of $Cu_{75}Al_{25}$ and $Cu_{71}Al_{25}Ni_4$

	$Cu_{75}Al_{25}$		$Cu_{75}Al_{25}Ni_4$	
	Position / 10^{-10} m	Area	Position / 10^{-10} m	Area
1st sub-peak	2.35	0.87	2.43	1.42
2nd sub-peak	2.56	3.86	2.65	3.80
3rd sub-peak	2.81	2.58	2.90	2.79
4th sub-peak	3.18	4.46	3.32	3.82

position of this sub-peak (2.35 Å), however, is less than the sum of the atomic radii of Cu(1.28 Å) and Al(1.43 Å) by about 0.35 Å, suggesting a strong interaction between Cu and Al. The area of the first sub-peak increases with addition of Ni. This suggests Ni can strengthen interaction between Cu and Al. the peak positions of the second sub-peak (2.56 Å) and the third sub-peak (2.81 Å) are close to the expected Cu-Cu distance (2.56 Å) and Al-Al distance (2.86 Å), respectively.

Under normal conditions, different metals and alloys have different reasons that cause the appearance of pre-peak[11~15]. For example, the pre-peak of K-Pb is thought to be caused by the phase transformation, while the pre-peak of Au-Ge alloys is caused by heteroatomic associates of composition Au_4Ge. So it is believed that the pre-peak of $Cu_{75}Al_{25}$ is related to formation of β-phase-like clusters due to strong Cu-Al chemical bond in liquid, manifesting character of medium-range order. The detail about β-phase-like clusters in the melt was published elsewhere[16]. The melt is considered to consist of the clusters regions and disorder atomic ones. After Ni added, Ni replaces partial Cu atoms and also form strong chemical bond with the around Al atoms in clusters. This causes the Cu-Al-Ni alloy further to develop a certain covalent characteristic that is favorable to form big clusters. At low quenching temperature, large quantities of atoms exist in clusters and the size of clusters is big and the amount of clusters is enormous in melt. During quick solidification, β phases develop from incorporating and growing of the clusters. therefore β phases with less fault come into being and the distribution of Ni in β phases is uniform. Ni can effectively restrain the diffusion of Cu and Al[17], so the precipitation of γ_2 can be suppressed. This is the reason why the Vickers hardness is low in ribbons fabricated at low liquid quenching temperature, as curve is shown in Fig. 2. Ni can operate similarly during the aging. This is the reason why the point at which the hardness begins to rise and shifts to higher temperature when the quenching temperature was decreased. When the deposition of the γ_2 cannot be suppressed at higher temperature, the hardness begins to increase, as shown in Fig. 3. The ordering reaction, $\beta \rightarrow \beta_1$ (Cu_3Al: DO_3), occurs at low temperature during quenching. Because of indiffusion of martensitic transformation, thermoelastic martensite must inherit atom order state of parent phase. β phases developed from the big β-phase-like clusters are very favorable to formation of high order degree β_1 phases. This is the reason why the order degree of martensite is high in ribbons fabricated at low liquid quenching temperature, as shown in Fig. 1 and Table 1, which is reverse in ribbons fabricated at high liquid quenching temperature. The precipitation of γ_2 also can be suppressed by higher cooling rate as curve 2 shown in Fig. 2.

[REFERENCES]

[1] Bubley I R, Koval Y N, Titov P V. β_1-γ transformation in Cu-Mn-Al alloys after low temperature aging [J]. Scr Met, 1999, 41: 637-641.

[2] Nagarjuna S, Srinivas M, Balasubramanian K, et al. Influence of polycrystalline grain size on yield and flow stress in Cu-1.5% Ti alloy [J]. Scr Met, 1994, 30: 1593-1597.

[3] Wei Z G, Peng H Y, Zou W H, et al. Aging effects in a $Cu_{12}Al_5Ni_2Mn_1Ti$ shape memory alloy [J]. Metall Trans A, 1997, 28: 955-967.

[4] Kainuma R, Takahashi S, Ishida K. Thermoelastic martensite and shape memory effect in ductile CuAlMn alloys [J]. Metall Trans A, 1996, 27: 2187-2190.

[5] Anantharaman T R, Suryanarayana C. Rapidly Solidified Metals [M]. USA: TRANS TECHPUBLICATIONS, 1987. 80-86

[6] Waseda Y. The Structure of Non-Crystalline Materials [M]. New York: McGRAW-HILL, 1980. 10-62

[7] Giessen B C. Liquid Metalls [M]. New York: Marcel Dekker Inc, 1972. 652.

[8] QIN J Y, BIAN X F, WANG W M, et al. Pre-peak on the structure of liquid hypoeutectic Al-Fe alloy [J]. Chinese Science Bulletin, 1998, 43(14): 1219-1224.

[9] WANG Wei-min, BIAN Xiu-fang, QIN Jing-yu. The atomic structure change in Al-16 pct Si alloy above the liquids [J]. Metall Trans A, 2000, 31: 2163-2168.

[10] WANG Ying-hua. Technological Basis for X-Ray Diffraction (in Chinese) [M]. Beijing: Atomic Energy Press, 1993. 263-332.

[11] Cervinka L. Several remarks on the medium-range order in glasses [J]. J Non-Cryst Solids, 1998, 132-134: 1-17.

[12] Manh D N, Mayu D, Pasture A, et al. Electronic structure and hybridization effects in transition-metal-polyvalent-metal alloys [J]. J Phys F: Met Phys, 1985, 15: 1911-1917.

[13] Vateva E, Savova E. New medium-range order features in Ge-Sb-S glasses [J]. J Non-Cryst Solids, 1995, 192-193: 145-149.

[14] Saboungi M L, Bioquist R, Volin K J. Structure of liquid equiatomic potassium-lead alloy: A neutron diffraction experiment [J]. J Chem Phys, 1987, 87(4): 2278-2281.

[15] Hoyer W, Jodicke R. Short-range and medium-range order in liquid Au-Ge alloys [J]. J Non-Cryst Solids, 1995, 193: 102-105.

[16] PAN Xue-min, BIAN Xiu-fang, QIN Jing-yu. Medium-range order structure clusters in Cu-12% Al alloys melt [J]. Acta Phys Chim Sin, 2001, 17(8): 708-712.

[17] Sun Y S, Lorimer G W, Ridley N. Microstructure and its development in Cu-Al-Ni alloys [J]. Metall Trans A, 1990, 21: 575-579.

(Edited by HUANG Jin-song)